ISSN 0965-545X, Polymer Science, Ser. A, 2014, Vol. 56, No. 1, pp. 83–89. © Pleiades Publishing, Ltd., 2014.

COMPOSITES

Effect of Montmorillonite Treatment with Supercritical CO_2 on the Morphology and Properties of Polypropylene Nanocomposites[1]

L. G. Furlan[a], S. A. Liberman[b], M. A. S. Oviedo[b], E. Cassel[c], and R. S. Mauler[d]

[a]*Federal Institite of Rio Grande do Sul, IFRS, Campus Restinga, Rua 7121, nº 285, Porto Alegre, 91791-501, Brazil*

[b]*Braskem S.A., III Pólo Petroquímico, Via Oeste, Lote 5, Triunfo, 95853-000, Brazil*

[c]*Chemical Engineering Department, Laboratório de Operações Unitárias, PUCRS, Av. Ipiranga, 6681, Porto Alegre, 90619-900, Brazil*

[d]*Chemistry Institute, Federal University of Rio Grande do Sul, UFRGS, Av. Bento Goncalves, 9500, Porto Alegre, 91501-970, Brazil*

e-mail: mauler@iq.ufrgs.br

Received July 20, 2012;
Revised Manuscript Received February 7, 2013

Abstract—The effects of montmorillonite (MMT) treatment with supercritical carbon dioxide (SC–CO_2) on clay morphology and the properties of polypropylene nanocomposites were investigated by wide-angle X-ray diffraction, transmission electron microscopy, scanning electron microscopy, dynamic mechanical analysis, and differential scanning calorimetry. The use of poly(propylene glycol) (PPG) was evaluated. The results showed that the MMT morphology (structure formation, dispersion, and orientation) was affected by treatment with SC–CO_2, and the use of PPG, or the use of CO_2 in the liquid state. Consequently, different reinforcement measurements were obtained. The relationship between structure and properties was reported.

DOI: 10.1134/S0965545X13090071

INTRODUCTION

Polymer nanocomposites have drawn a great deal of interest in recent years due to their high potential property improvement compared with pristine polymer or conventional micro and macro-composites [1–5]. In particular, the polypropylene/montmorillonite (PP–MMT) is able to conjugate relatively low cost and extraordinary versatility, properties that are very attractive mainly for the industrial market. The great advantage of clay nanocomposites over traditional composites (talc, glass, carbon fibers, etc.) is the relatively low amount of nanoparticles dispersed in the polymer matrix [6–9] capable to improve mechanical properties [10–17]. However, key challenges in the production of polymer-based nanocomposites, and the major technological barrier to achieve superior properties, center around the difficulty of dispersing the filler uniformly in a host matrix. Exfoliated silicate layers are supposed to create large polymer-clay interfaces in nanocomposites, leading to a large extent of reinforcement at very low silicate contents [18]. Therefore, it would be advantageous to develop methods that help to increase the extent of nanoclay dispersion. In this context, the study of supercritical fluids (SCF) and their application in industrial processes have gained much interest over the last years, as they can be used as environmentally friendly solvents for a range of materials synthesis or modification. Many processes based on supercritical fluids [19–22] have been successful used in nano-materials applications [23–26]. In particular, supercritical carbon dioxide (SC–CO_2) has become in evidence due to its special characteristics and many desirable attributes such as low cost, abundance, no flammability, low toxicity, greater diffusion, and penetration into bulk materials or normal liquids. In nanocomposite preparation [20], two approaches for the application of SCF have received special attention: in situ polymerization using SCF, and continuous melt extrusion [24]. It has been reported that the presence of SC–CO_2 promotes a significant increase in the basal spacing of the clay, and thereby may enhance the polymer intercalation into the galleries of the clay in extrusion processes [20]. Another alternative and efficient method is the treatment of the filler with SC–CO_2 in a previous step of mixing the polymer with the clay. The SC–CO_2 diffuses between the clay galleries and it is possible, for example, that materials such as *n*-dodecylamine [27], poly(ethylene oxide) [28], 4-phenylazoaniline [29] and can be easily introduced into nanolayers in the presence of SC–CO_2. This method consists of immersing the layered clays in supercritical CO_2 for a certain time at a preset temperature and pressure fol-

[1] The article is published in the original.

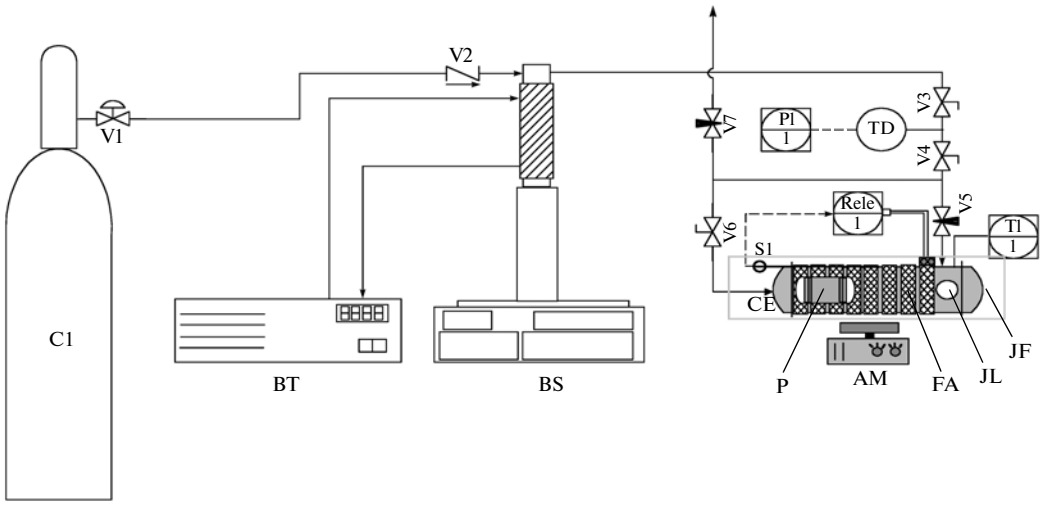

Fig. 1. Schematic diagram of the experimental apparatus: C1—gas reservoir, BS—syringe pump, CE—high pressure cell, JL, JF—sapphire windows, AM—magnetic stirrer, TD—pressure transducer, FA—electrical device, PI—pressure indicator; V1–V7—valves, S1—thermocouple, IT—temperature indicator, BT—thermostatic bath.

lowed by rapid depressurization [30, 31]. The resultant nanocomposites had significant enhancements in the rheological properties, and showed a characteristic of dispersed MMT with good polymer-clay interactions [32]. In this context, the aim of this work is to explore the treatment of MMT clay with SC–CO_2, and to evaluate its effects on PP-nanocomposite properties.

EXPERIMENTAL

Materials

A commercial grade polypropylene (Braskem SA., Brazil) with a melt flow index (MFI) of 3.5g/10 min (230°C/2.16 kg) was used. The commercial montmorillonite (MMT) Cloisite 15A, modified with a quaternary ammonium salt [organic modifier = $R_2N^+(HT)_2$; R = methyl group and HT is hydrogenated tallow (~65% C18; ~30% C16; ~5% C14)], with a cation exchange capacity (CEC) of 125 meq/100 g from Southern Clay Products, and poly (propylene glycol) (PPG) ($M_w = 10^3$), were used as received.

Clay Treatment with SC–CO_2

The clay and SC–CO_2 mixture were prepared in a high-pressure variable-volume view cell (Fig. 1), which consists of a view cell with three sapphire windows for visual observation, an absolute transducer (Smar LD 301) with an accuracy of 0.12 bar, a pressure indicator (Smar HT2) for the pressure data acquisition, and a high-pressure pump syringe (ISCO 260D). The maximum internal volume of the view cell was 20 cm^3, and it contained a movable piston, which permits for pressure control inside the cell. Heating tapes were used throughout the apparatus to maintain constant temperature in the extraction section. A PID temperature controller was connected to a thermocouple PT-100 with an accuracy of 0.1, which was in direct contact with the mixture inside the cell body.

The pure clay or the moisture clay-PPG (clay/PPG = 2/1 wt/wt) was loaded into the cell, and the solvent was pumped into the cell until reaching the experimental pressure and temperature (180 bar/60°C, 140 bar/50°C with and without PPG). It is important to note that at 180 bar/25°C, CO_2 is in the liquid state. The solvent charge was monitored by the change in the volume of the transfer vessel of the high-pressure pump. After 24 h, the system was rapidly depressurized to atmospheric pressure.

Preparation of PP-Nanocomposites

Samples of polypropylene and 2 wt % of montmorillonite treated in different SC–CO_2 conditions (Table 1) were prepared using a Haake Rheomix 600 at 180°C, 60 rpm for 7 minutes.

Analytical Techniques

Wide-angle X-ray diffraction (WAXD) experiments were performed in a Siemens D-500 diffractometer using CuK_α radiation to characterize the clay before and after treatment with SC–CO_2. The d-spacing (basal distance between clay layers) values were calculated using Bragg's Law. The clay morphology was studied using a scanning electron microscope (JEOL JSM 5800).

Nanocomposite samples for testing were obtained by melting compressed films at 190°C, for 2 min, using 0.7 kgf. The thermal and crystallization behaviors of the nanocomposites were studied by differential scanning calorimetry (DSC) using a 2100 Thermal

Table 1. Image analysis results of PP–MMT (2 wt %) nanocomposites

Sample	SC–CO_2-MMT treatment conditions	Average number of particles/170 μm^2	Average aspect ratio
1	Untreated	39	7
2	140 bar/50°C	32	7
3	180 bar/60°C	38	8
4	180 bar/25°C	78	12
5	140 bar/50°C/PPG	68	8
6	180 bar/60°C/PPG	44	9

Analyst Instruments, where linear heating and cooling experiments were made at 10 deg/min under a constant flow of nitrogen, and calibrated with an indium standard. The melting temperature T_m was obtained on the second heating curve.

Transmission electron microscopy (TEM) was performed using ultra thin cuts obtained from the compressed specimens using a JEOL JEM-120 EXII TEM microscope, operating at an accelerating voltage of 80 kV. The cuts were placed on 300 mesh Cu grids. Ultra thin sections (50 nm thickness) of the specimens were obtained by cryoultramicrotomy with a diamond knife at –80°C. The particle analyses were performed by the use of an image editor (PhotoDraw 2000, Microsoft Corporation). The original gray scale images were converted into black and white images in order to provide the identification of particles by the image analysis program. Agglomerates, intercalated structures, and isolated platelets are treated as single particles in this process. The image analysis program (ImageTool 3.0, UTHSCSA) created files with the thickness and length of each particle.

Dynamical mechanical analysis (DMA) was performed in a dynamic-mechanical analyzer TA Instrument model Q800. The storage modulus was determined using a tension film clamp from –30 to 130°C at 3 deg/min.

RESULTS AND DISCUSSION

MMT Morphology

Figure 2 shows the WAXD difractograms of the MMT treated at different SC–CO_2 conditions. No differences in interlayer spacing (3.27 nm) were observed in the treated SC–CO_2 samples compared to the untreated MMT. On the other hand, a decrease in the peak intensity (maximum of 35%) was observed. This behavior can be attributed to the reduction in tactoids size, especially when higher pressure and temperature were used. A similar observation was reported when other fillers were processed with SC–CO_2 [32]. When the PPG were used, the 2θ values confirm the increase in basal distance d from 3.27 to 3.99 nm, independent of the pressure/temperature conditions. This observation indicates that the PPG intercalates into the MMT layers.

The morphology of the MMT before and after supercritical processing was evaluated by SEM

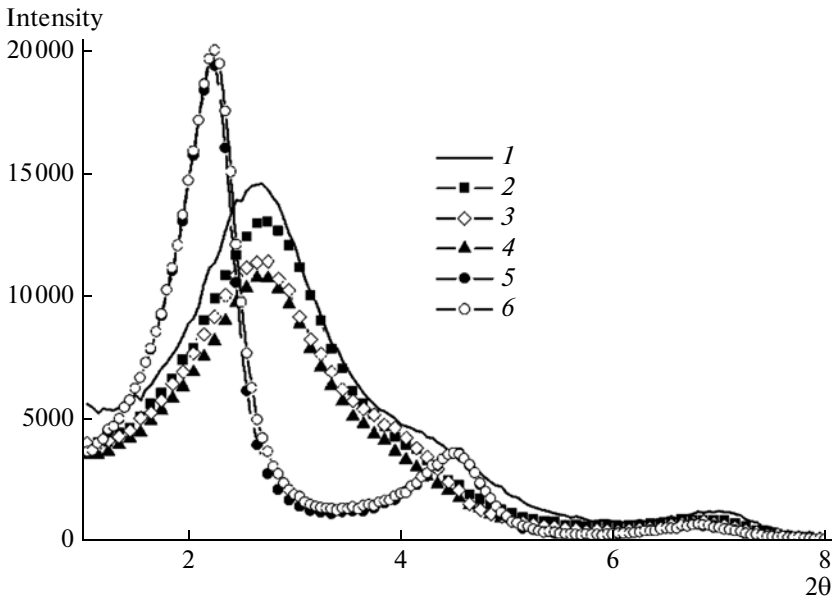

Fig. 2. WAXD of MMT treated in different SC–CO_2 conditions: (*1*) untreated, treated at (*2*) 140 bar/50°C, (*3*) 180 bar/25°C, (*4*) 180 bar/60°C, (*5*) 140 bar/50°C/PPG, and (*6*) 180 bar/60°C/PPG.

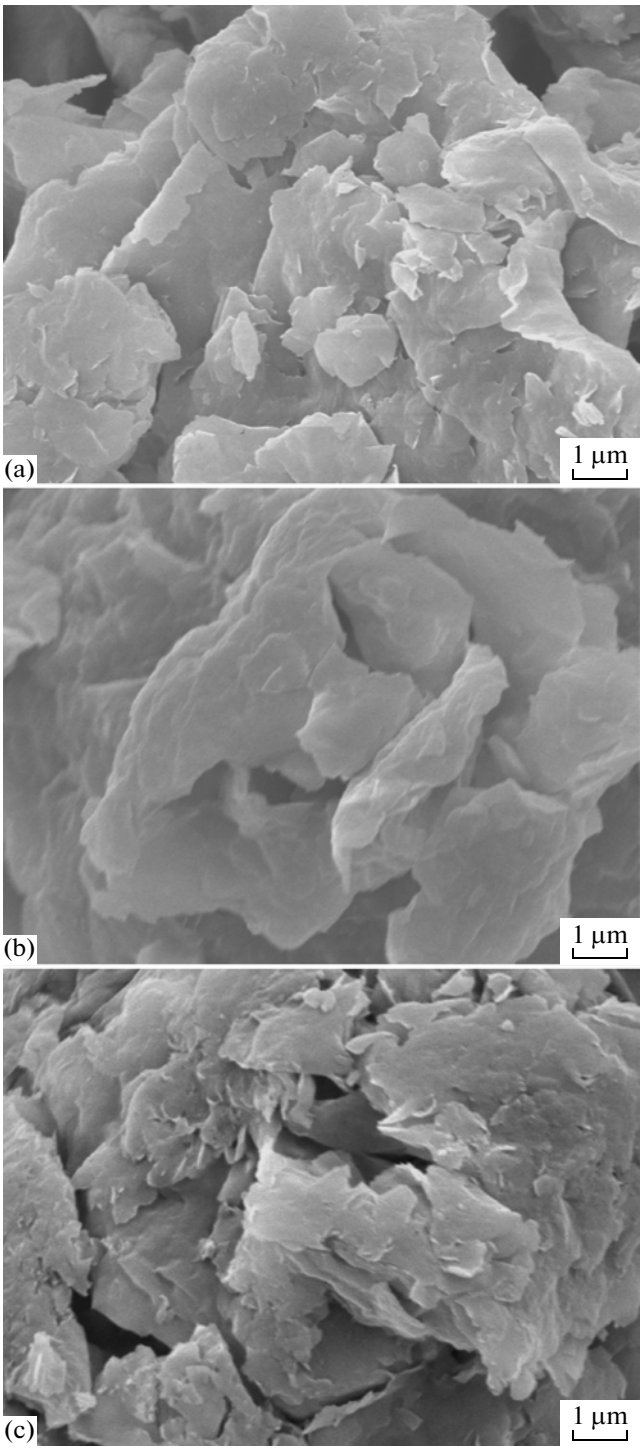

Fig. 3. SEM images of MMT (a) untreated and SC–CO_2 treated at (b) 180 bar/60°C/PPG and (c) 180 bar/60°C.

microscopy (Fig. 3). When the PPG was used, the images suggested the reduction of the number of smaller particles. On the other hand, in the absence of PPG (Fig. 3c) the particle layers seemed to be delaminated, and the larger particles fractured into smaller particles during supercritical processing.

PP–MMT Nanocomposite Morphology

Nanocomposites prepared with MMT processed with SC–CO_2 presented distinct morphologies that were dependent on the experimental conditions and the presence of PPG. Figure 4 shows representative TEM micrographs. In particular, some aggregates of MMT platelets were found using the untreated MMT, indicating a poor degree of intercalation or exfoliation. The MMT treated in the absence of PPG showed uniform dispersion and more aligned tactoids with different particle dimensions and dispersion. The increasing of particle number, with no agglomerated particles, is clear in the sample prepared with clay treated at 180 bar/25°C (CO_2 on liquid state). This behavior suggests that the higher viscosity of CO_2 in the liquid state improves the dispersion process of the MMT. Furthermore, at 180 bar/60°C and 140 bar/50°C, intercalated structures were observed with distinct characteristics. Larger and shorter (180 bar/60°C), and some curved structures (140 bar/50°C) were found. On the other hand, the MMT samples processed with PPG also showed a good degree of dispersion, and some heterogeneity with large agglomerates and some short particles, mainly at 180 bar/60°C/PPG. From the TEM images, it is clear that the PPG intercalation in the clay decreases the final clay orientation.

The quantitative analysis of the number of dispersed clay particles was determined by image analyses, and the aspect ratio was calculated as the relationship between the average length and the average thickness of the particle. As shown in Table 1, an increase in the average particle number is observed only at 180 bar/25°C and at 140 bar/50°C/PPG. An increase in the average aspect ratio is found in the samples treated with PPG at 180 bar/25°C.

Particle aspect ratio histograms (Fig. 5a) show an increase in the population of particles with an aspect ratio > 12 for clay treated at 180 bar/25°C. The larger aspect ratios for the dispersed clay produced at these conditions reflect a combination of two effects: higher platelet length, and a decrease in thickness. On the other hand, when the MMT was treated at 180 bar/60°C and at 140 bar/50°C, a high population (superior to 70%) of particles at low aspect ratio values (3 to 12) was found. For the samples processed with PPG (Fig. 5b), it is clear the increase in the aspect ratio population when higher pressure and temperature were used.

PP–MMT Nanocomposite Properties

Table 2 shows the effect of clay treatments on the thermal properties of PP nanocomposites. The melting temperature T_m increased compared to pure PP for the nanocomposites. The crystallization temperature T_c increased slightly only when PPG were used, independent of the experimental conditions. The cristal-

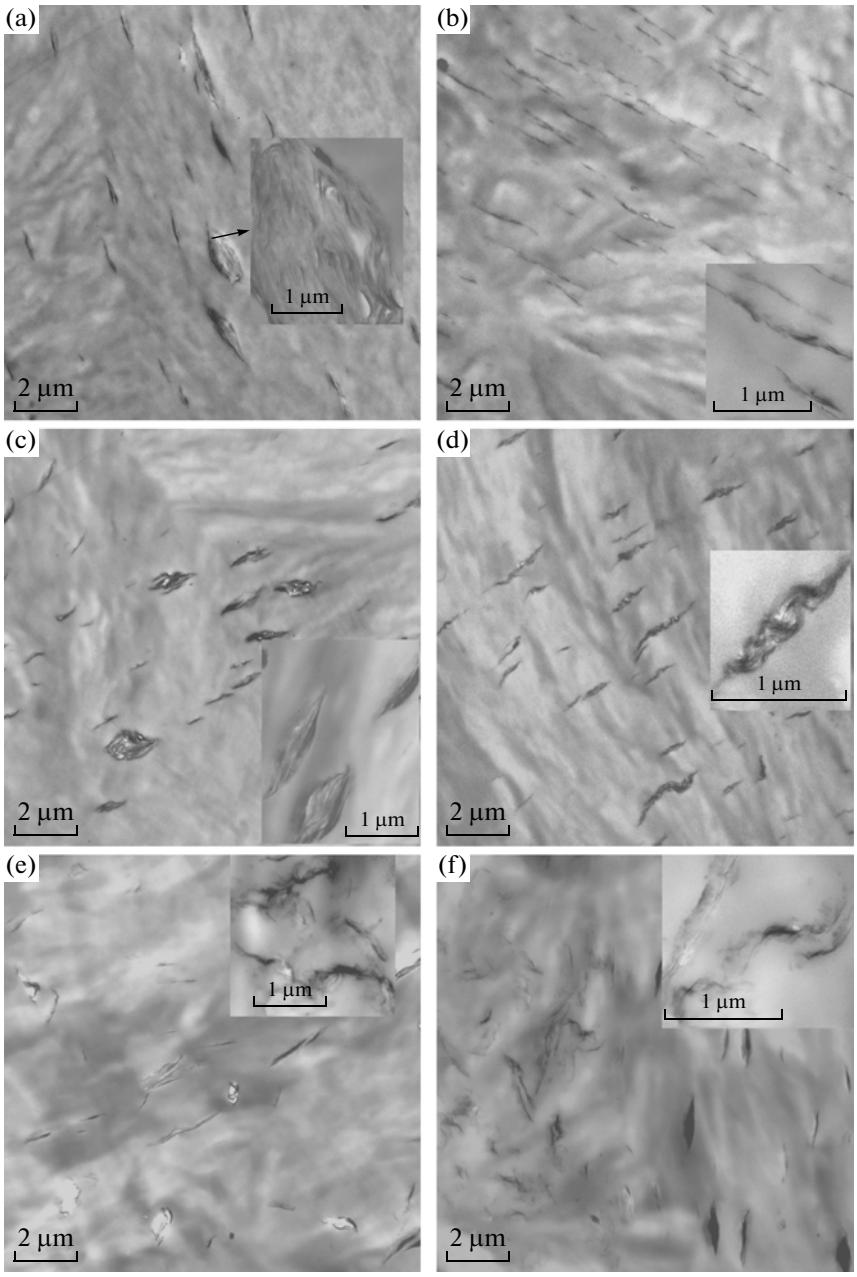

Fig. 4. TEM micrographs of PP–MMT nanocomposites produced by: (a) untreated MMT and MMT treated at different SC–CO_2 conditions: (b) 180 bar/25°C, (c) 180 bar/60°C, (d) 140 bar/50°C, (e) 180 bar/60°C/PPG, and (f) 140 bar/50°C/PPG.

linity χ (%) of the nanocomposites did not change with the MMT treatment. On the other hand, reduction of the T_g values (to 1°C) in absence of PPG at 180 bar/25°C reveals a behavior similar to the plasticizing effect, probably due to the poor interfacial adhesion (PP-clay) by absence of compatibilizing agent. In the others systems, the T_g values were unaffected.

The MMT treatment influences the PP-nanocomposite reinforcement and it is reflected in the storage modulus measurements E'. As shown in DMA curves (Fig. 6) and E' at 23°C (Table 2), the E' values of PP–clay (2%) are higher than that of unfilled PP, indicating that the incorporation of clay into the PP matrix has good reinforcing effects. It is important to point out the relationship between the reinforcement properties and the morphological aspects: the results strictly depend on the filler dispersion and the type of dispersion obtained in the polymer matrix promoted by SC–CO_2 treatment at different conditions. In the absence of PPG, the highest reinforcement of nanocomposites is evident, being 180 bar/60°C > 140 bar/50°C > 180 bar/25°C. The E' is related to the

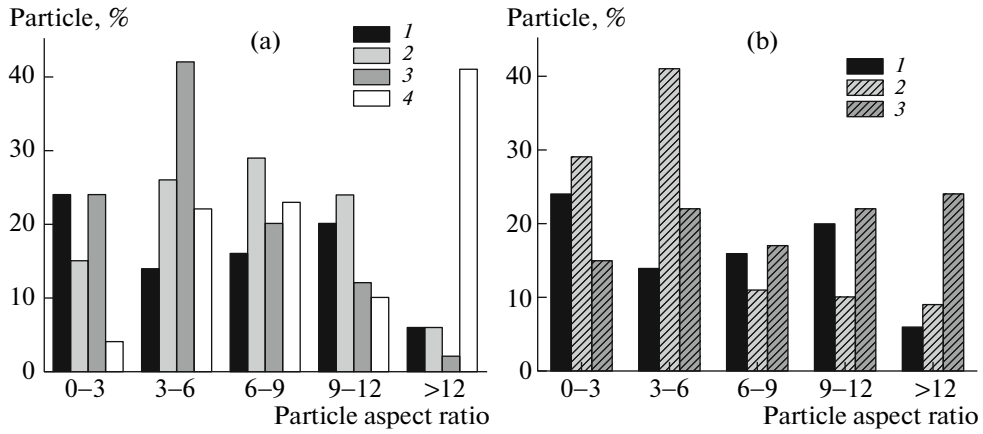

Fig. 5. Comparison of particle aspect ratio of nanocomposites prepared with MMT SC–CO_2 processed in (a) the absence of PPG or (b) with PPG. SC–CO_2 conditions: (*1*) untreated, treated at (*2*) 140 bar/50°C, (*3*) 180 bar/60°C, and (*4*) 180 bar/25°C. The results were obtained by software image analysis of the micrographs. Number of analyzed particles: (*1*) 79, (*2*) 129, (*3*) 125, and (*4*) 212.

clay morphology, which suggested that the higher *E*' occurs in the presence of intercalated structures. On the other hand, the poor *E*' performance of the MMT treated at 180 bar/25°C was observed despite there being well dispersed particles. In this case, intercalated structures are not observed, and the MMT particles seem to have a similar plasticizer effect for PP caused by the weak interaction PP–MMT. These results are the opposite of other systems containing compatibilizing agents, ex. PP–*g*–MA [10], where more exfoliated systems containing higher aspect ratios lead to an increase in the reinforcement by improvements on the interfacial adhesion.

As shown at Fig. 6, when PPG is used, the storage modulus is similar to that of untreated MMT, independent of the SC–CO_2 condition. Although the dispersion and the aspect ratio values increased in comparison with untreated MMT, these factors do not seem to influence the *E*' performance of the nanocomposites. In this case the poor reinforcement effect, in comparison to systems without PPG, was determined probably by a decrease in clay particle orientation. The disorganized structures formed when PPG was used were fundamental for the reinforcement effect. In general, the results appointed that SC–CO_2 treatment of the MMT increased the dispersion of the MMT in the PP matrix. However, if the orientation of MMT structures is not efficient, the result will be a loss in mechanical property.

CONCLUSIONS

This work showed the influence of SC–CO_2 treatment on clay morphology and PP–MMT nanocomposite properties. Changes on the nanocomposite morphology (structure formation, dispersion, and orientation) strictly depend on the CO_2 processing conditions, and the use of PPG. Consequently, different reinforcement measurements were obtained, and the best performance was obtained when the MMT was treated with SC–CO_2 at higher pressure and tempera-

Table 2. PP–MMT (2 wt %) nanocomposites properties

Sample	SC–CO_2 MMT treatment conditions	*E*', MPa (23°C)	T_g, °C	T_m, °C	T_c, °C	χ, %
PurePP	–	247	11	161	113	49
1	Untreated	1208	7	165	113	41
2	140 bar/50°C	1570	9	163	114	48
3	180 bar/60°C	2143	8	164	113	44
4	180 bar/25°C	668	1	164	113	47
5	140 bar/50°C/PPG	1111	12	164	116	47
6	180 bar/60°C/PPG	1264	13	164	116	47

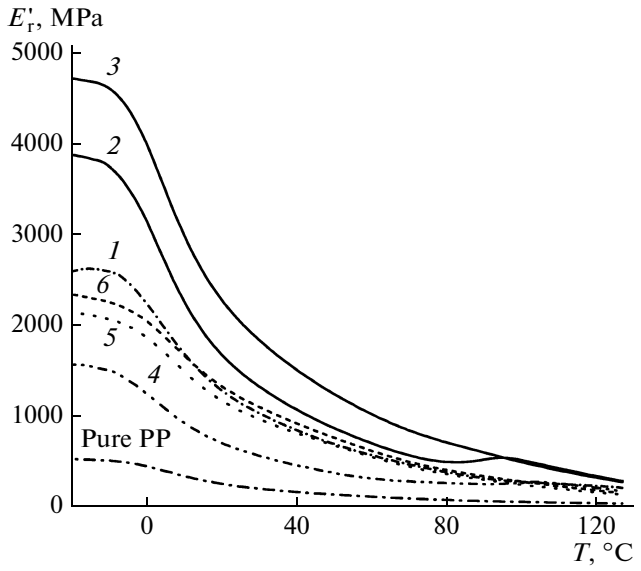

Fig. 6. Storage modulus curves of pure PP and PP–MMT nanocomposites (2 wt %): (*1*) untreated and SC–CO_2 treated at 140 bar/50°C (*2*), 180 bar/60°C (*3*), 180 bar/25°C (*4*), 140 bar/50°C/PPG (*5*) and at 180 bar/60°C/PPG (*6*).

tures. The presence of PPG reveals a smaller reinforcement due to the poor MMT orientation in the PP matrix. The MMT treated with CO_2 in its liquid state showed a reduction in intercalation, and an increase in dispersion. However, this factor was not significant for a storage modulus gain.

ACKNOWLEDGMENTS

The authors thank Braskem S.A., CNPq, FAPERGS/Pronex, and Finep for financial and technical support.

REFERENCES

1. S. Ray and M. Okamoto, Prog. Polym. Sci. **28**, 1539 (2003).
2. M. Alexandre and P. Dubois, Mater. Sci. Eng. **28**, 63 (2000).
3. F. Hussain, M. Hojatti, M. Okamoto, and R. Gorga, J. Compos. Mater. **40**, 1511 (2006).
4. M. Okamoto, Mater. Sci. Technol. **22**, 777 (2006).
5. L. J. Lee, C. Zeng, X. Cao, X. Han, J. Shen, and G. Xu, Compos. Sci. Technol. **65**, 2344 (2005).
6. S. G. Lei, S. V. Hoa, and T. Ton-That, Compos. Sci. Technol. **66**, 1274 (2006).
7. L. B. Paiva, A. R. Morales, and T. R. Guimares, Mater. Sci. Eng. A **447**, 261 (2007).
8. J. H. Kim, C. M. Koo, Y. S. Choi, K. H. Wang, and J. J. Chung, Polymer **45**, 719 (2004).
9. P. Maiti, N. H. Nam, and M. Okamoto, Macromolecules **3**, 2042 (2002).
10. F. Perrin-Sarazin, M. T. Ton-That, M. N. Bureau, and J. Denault, Polymer **46**, 11624 (2005).
11. L. Százdi, B. Pukánszky, G. J. Vancso, and B. Pukánszky, Polymer **47**, 4638 (2006).
12. E. Manias, A. Touny, L. Wu, K. Strawhecker, B. Lu, and T. C. Chung, Chem. Mater. **13**, 3516 (2001).
13. P. C. LeBaron, Z. Wang, and T. J. Pinnavaia, Appl. Clay Sci. **15**, 11 (1999).
14. J. W. Lee, Y. T. Lim, and O. Park, Polym. Bull. (Berlin) **45**, 191 (2000).
15. C. Ding, D. Jia, H. He, B. Guo, and H. Hong, Polym. Test. **24**, 94 (2005).
16. K. Krump, A. S. Luyt, and I. Hudec, Mater. Lett. **60**, 2877 (2006).
17. C. M. Koo, S. O. Kim, and J. Chung, Macromolecules **36**, 2748 (2003).
18. R. A. Vaia, G. Price, P. N. Ruth, H. T. Nguyen, and J. Lichtenhan, Appl. Clay Sci. **15**, 67 (1999).
19. S. P. Nalawade, F. Picchioni, and L. P. M. Janssen, Prog. Polym. Sci. **31**, 19 (2006).
20. D. L. Tomasko, X. Han, D. Liu, and W. Gao, Curr. Opin. Solid State Mater. Sci. **7**, 407 (2003).
21. P. Svoboda, K. Trivedi, D. Svobodova, K. Kolomaznik, and T. Lee, Polym. Test. **31**, 444 (2012).
22. E. Naveau, C. Calberg, C. Detrembleura, C. Jrme, and M. Alexandre, Appl. Clay Sci. **51**, 467 (2011).
23. Y. Haldoraia, J. Shima, and K. Limc, J. Supercrit. Fluids **45**, 71 (2012).
24. C. Chen and D. Baird, Polymer **53**, 4178 (2012).
25. K. S. Morley, P. C. Marr, P. B. Webb, A. R. Berry, F. J. Allison, G. Moldovan, P. D. Brown, and S. M. Howdle, J. Mater. Chem. **12**, 1898 (2002).
26. M. F. Mendes and G. L. V. Coelho, Adsorption **11**, 139 (2005).
27. T. P. Shi1, K. Yao, S. Nishimura, Y. Imai, N. Yamada, and E. Abe1, Chem. Lett. **31**, 440 (2002).
28. Q. Zhao and E. T. Samulski, Macromolecules **36**, 6967 (2003).
29. R. Ishii, H. Wada, and K. Ooi, J. Colloid Interface Sci. **254**, 250 (2002).
30. G. K. Serhatkulu, D. Dilek, and E. Gulari, J. Supercrit. Fluids **39**, 264 (2006).
31. Q. T. Nguyen and D. G. Baird, Polymer **48**, 6923 (2007).
32. S. Horsch, G. K. Serhatkulu, E. Gulari, and R. M. Kannan, Polymer **47**, 7485 (2006).